Single-crystalline orthorhombic molybdenum oxide nanobelts: synthesis and photocatalytic properties†

Yuping Chen, Chunliang Lu, Lin Xu, Ying Ma, Wenhua Hou* and Jun-Jie Zhu*

Received 13th January 2010, Accepted 11th May 2010
DOI: 10.1039/c000744g

Single crystalline MoO_3 nanobelts with width of 200–300 nm and the length up to several tens of micrometres were prepared by a facile hydrothermal method and characterized. Based on time- and temperature-dependent experiments, a solid–solution–solid transformation mechanism was proposed for the formation of crystalline MoO_3 nanobelts. The as-prepared MoO_3 nanobelts were used as a photocatalyst to degrade methylene blue (MB) under visible light irradiation and demonstrated a dramatic activity, indicating that the as-prepared MoO_3 nanobelts were promising candidates for the photodegradation of organic dyes. A self-sensitization photocatalytic mechanism was suggested based on the experimental results.

1. Introduction

Photocatalysis with solar energy and semiconductors is of great importance in solving global energy and environment issues.[1–3] Many semiconductors such as TiO_2, ZnO, WO_3, CdS and NiO have been tested as photocatalysts, and it is generally accepted that TiO_2 is the most reliable material due to its low cost, non-toxicity and stability under irradiation. However, its poor natural light absorption capability due to its intrinsically large energy band gap (~3.2 eV) and the poor quantum yield caused by the rapid recombination of photogenerated electrons and holes significantly limit the broad application of TiO_2 for photovoltaics and photocatalysts.[4–8] Therefore, developing novel visible light-responsive photocatalysts with high activity and stability seems to be necessary from the viewpoint of using solar energy. Recently, a series of layered materials such as nanosheets of $K_4Nb_6O_{17}$, $HTiNbO_5$, HNb_3O_8, $HCa_2Nb_3O_{10}$ and $Ba_5Ta_4O_{15}$ have attracted great attention due to their photoactive properties and potential applications.[9–13] The large inner surface of these layered materials may potentially be available for various catalytic reactions after the reactant molecules can be intercalated into the interlayer. The intercalation can effectively promote photocatalytic reaction since the recombination of photogenerated electrons and holes is depressed by the electron transfer to the layered host. These results indicate possible application of layered materials in photocatalytic field.

Molybdenum trioxide (MoO_3), as a wide band gap n-type semiconductor, is one of the most intriguing transition metal oxides. It has been investigated over the past decades due to its distinctive properties of electrochromism, thermochromism and photochromism, as smart materials, gas sensors, catalysts and host materials for intercalation.[14–24] In addition, it has been found to be a good precursor for the synthesis of some important materials such as MoO_2, MoS_2, $MoSe_2$ and Mo, *etc.*[25–30] Molybdenum trioxide usually has three forms: the well-known thermodynamically stable orthorhombic MoO_3 (α-MoO_3), metastable monoclinic MoO_3 (β-MoO_3) and hexagonal MoO_3 (h-MoO_3). Among them, α-MoO_3 has attracted most attention because of its double-layered planar structure. The fundamental characteristics of one-dimensional α-MoO_3 nanostructures have been reported.[31–35] However, there remains much interest in the morphology-controllable synthesis and novel properties of α-MoO_3.[36] To the best of our knowledge, there is no report about investigation of the photocatalytic properties of α-MoO_3 nanobelts to degrade MB under visible light irradiation.

Herein, we report a novel route to synthesize single-crystalline α-MoO_3 nanobelts in the presence of TX-10 by a hydrothermal technique. A series of condition-dependent experiments were performed and a solid–solution–solid growth mechanism is proposed. The photocatalytic properties of α-MoO_3 nanobelts to degrade organic dyes such as MB under visible light irradiation are determined and a possible photocatalytic mechanism is suggested.

2. Experimental

2.1 Preparation of samples

All reagents were of analytical grade and used as received without further purification. Distilled water was used throughout. In a typical synthesis, 0.49 g ammonium heptamolybdate tetrahydrate ($(NH_4)_6Mo_7O_{24}\cdot 4H_2O$) was dissolved in 13 mL of distilled water under magnetic stirring. Then 7 mL 3 mol L^{-1} HNO_3 was added into the solution. After stirring for another 5 min, 100 μL TX-10 was added dropwise. The obtained transparent solution was transferred and sealed in a Teflon-lined stainless autoclave with a capacity of 50 mL. The autoclave was heated to 180 °C and held for 20 h, then allowed to cool to room temperature. The precipitate was washed several times with absolute ethanol and distilled water, respectively, and then dried at 60 °C for several hours and kept for further characterization.

Key Laboratory of Mesoscopic Chemistry of MOE and Key Laboratory of Analytical Chemistry for Life Science of MOE, School of Chemistry and Chemical Engineering, Nanjing University, Nanjing, 210093, P. R. China. E-mail: whou@nju.edu.cn; jjzhu@nju.edu.cn

† Electronic supplementary information (ESI) available: Additional figures (Fig. S1–S10). See DOI: 10.1039/c000744g

2.2 Characterization

The BET surface area was measured at 77 K by using a Micromeritics ASAP 2000 volumetric adsorption analyzer. All samples were characterized by powder X-ray diffraction (XRD) on a Philip-X'Pert X-ray diffractometer with monochromatized Cu Kα (λ = 1.5418 Å) incident radiation. The size distribution and morphology of all samples was analyzed by TEM observation on a JEOL JEM-200CX transmission electron microscope and SEM observation on a LEO 1530VP field emission electron microscope operated at an accelerating voltage of 8 kV. HRTEM images were taken using a JEOL 2010 microscope at an accelerating voltage of 200 kV. The components of MoO3 were confirmed with a VG ESCALAB MKIIX-ray photoelectron spectrometer. The binding energy (BE) was calibrated by setting the measured BE of C1s to be 284.6 eV. The UV-visible absorption spectroscopic measurements were performed on a Shimadzu UV-3600 spectrophotometer, using a quartz cell with a width of 1 cm. UV/vis reflectance spectroscopic measurements were performed on a Shimadzu UV-3600 spectrophotometer by dispersing the sample on BaSO4. Fourier transformed infrared spectroscopy (FT-IR) was acquired with a Nicolet 6700 FT-IR spectrometer using KBr pellets. Raman spectra were recorded on a Renishaw inVia Raman microscope (excited with an Ar+ line at 514 nm). The zeta-potential test was performed on a Nano-Z Zeta-potential instrument.

2.3 Photocatalytic properties

The photocatalytic activities were evaluated by measuring the photocatalytic degradation of MB in water under the illumination of visible light (λ > 420 nm). A 300 W tungsten halogen lamp with a 420 nm cutoff filter was used as the energy source for photoexcitation. In a typical degradation experiment, 100 mL methylene blue solution with a concentration of 10 mg L^{-1} and 50 mg as-prepared molybdenum oxide nanobelts were added into a 250 mL Pyrex beaker, and then stirred continuously in the dark for 30 min to ensure adsorption/desorption equilibrium. The equilibrium concentration of MB was used as the initial value for the photodegradation processes. At certain time intervals, 5 mL aliquots were sampled and centrifuged to remove the particles. The degradation of organic dye was monitored by measuring the absorbance of the aliquot solution using the UV-visible spectrophotometer with de-ionized water as reference. The characteristic absorption of MB at 664 nm was chosen as the parameter to be monitored for the photocatalytic degradation process.

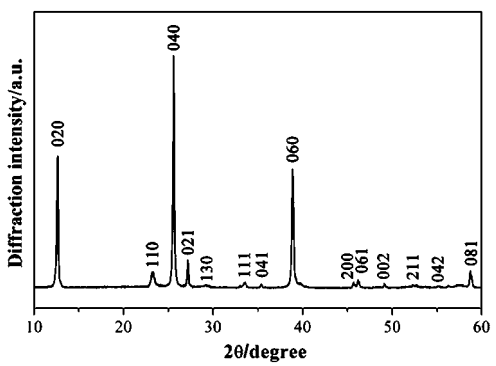

Fig. 1 XRD pattern of the as-synthesized MoO_3 nanobelts.

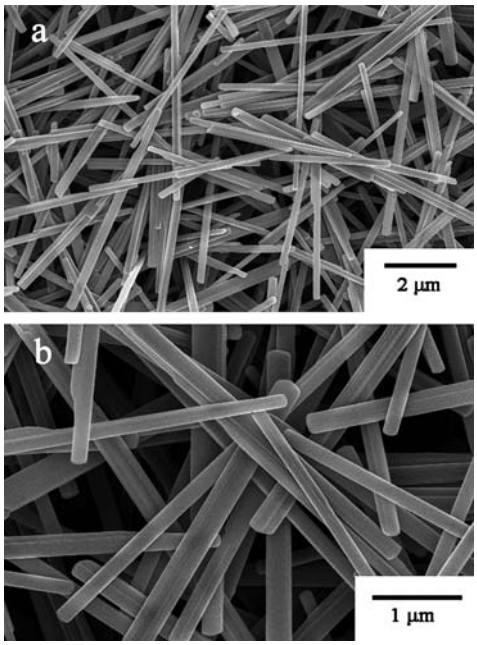

Fig. 2 Typical SEM images of the as-synthesized MoO_3 nanobelts: (a) low-magnification SEM image; (b) high-magnification SEM image.

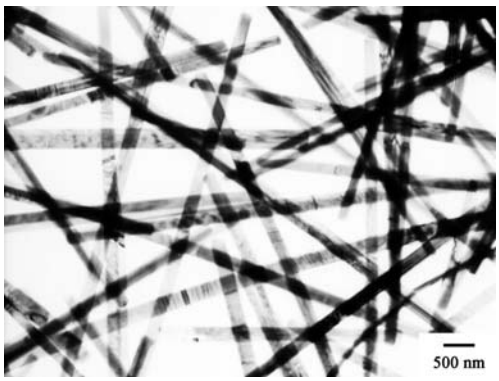

Fig. 3 Typical TEM image of the as-synthesized MoO_3 nanobelts.

3. Results and discussion

3.1 Characterization of molybdenum oxide nanobelts

The X-ray powder diffraction pattern of the as-prepared α-MoO_3 is shown in Fig. 1. All the diffraction peaks can be indexed to an orthorhombic phase of MoO_3 (JCPDS 35-0609, $a = 0.3963$ nm, $b = 1.3856$ nm, $c = 0.3697$ nm, space group *Pbnm*) and no characteristic peaks were observed for other impurities, indicating that pure α-MoO_3 was obtained. In addition, compared with the standard XRD result, the stronger intensity of the reflection peaks (02*k*0) indicates the anisotropic growth of the obtained α-MoO_3.[36,37]

Fig. 2 shows typical FE-SEM images of the α-MoO_3. A representative TEM image of MoO_3 nanobelts is shown in Fig. 3, which shows that the MoO_3 is composed of uniform nanobelts with width of 200–300 nm, thickness of 30–50 nm, and the length up to several tens of micrometres. Fig. 4 shows the HRTEM image of MoO_3 nanobelts. The selected area electron diffraction

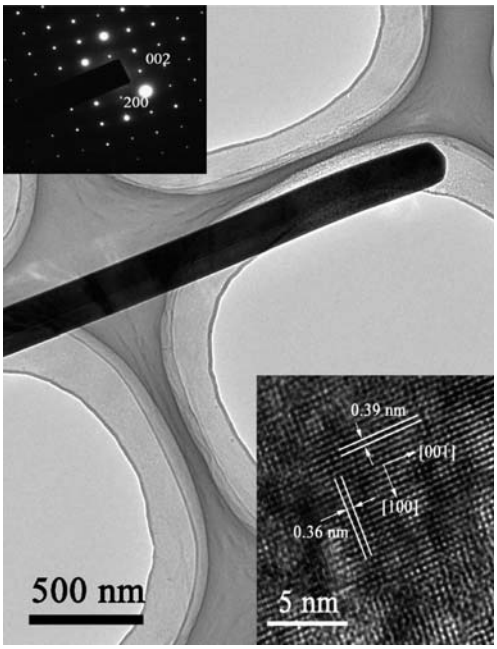

Fig. 4 Typical TEM image of the as-synthesized MoO_3 nanobelts (inset: selected area electron diffraction (SAED) pattern and HRTEM image of an individual molybdenum oxide nanobelt).

(SAED) pattern (inset of Fig. 4) recorded perpendicularly to the growth axis of a single nanobelt can be indexed to the [010] zone of α-MoO_3, implying preferential growth along the *c*-axis or [001] direction, which is consistent with XRD and HRTEM results. This demonstrates a high degree of crystallinity, while there is still some disorder, which might be introduced by the existence of oxygen vacancies. The interplanar spacing along the two different directions is determined to be 0.39 and 0.36 nm; the values are corresponding to d_{100} and d_{001} of the orthorhombic MoO_3 phase, respectively.

Fig. 5 typically depicts the XPS spectra of the as-synthesized MoO_3 nanobelts. Peaks of Mo 3d, Mo 2p, C 1s, O (KLL) and O 1s can be identified for MoO_3 nanobelts from Fig. 5a. In Fig. 5b, two Mo 3d peaks at 232.5 and 235.7 eV can be found for MoO_3 nanobelts, which is consistent with the previous report of Mo^{6+} and no apparent peak of Mo^{5+} or Mo^{4+} is observed,[38,39] indicating the main valance of molybdenum in the sample is +6. Therefore, the molecular formula of the as-prepared molybdenum oxide nanobelts can be expressed as $MoO_{3-\delta}$, where δ represents the number of oxygen vacancies. The XPS spectrum of O 1s is shown in Fig. 5c and can be separated into two peaks. The peak centered at 529.6 eV is associated with the O^{2-} ions in the orthorhombic MoO_3, and the peak at 530.5 eV is associated with the O^{2-} ions in the oxygen deficient regions within the matrix of MoO_3, respectively.[40,41]

FT-IR was performed to investigate chemical bonding states between molybdenum and oxygen atoms in the MoO_3 nanobelts. Fig. 6 shows the FT-IR spectrum of MoO_3 nanobelts measured in the 4000–400 cm^{-1} region. It can be seen that the as-prepared nanobelts mainly show five peaks at 553, 876, 995, 1630 and 3445 cm^{-1}, respectively. The peak at 995 cm^{-1} is due to the terminal Mo=O bond, which is an indicator of the layered orthorhombic

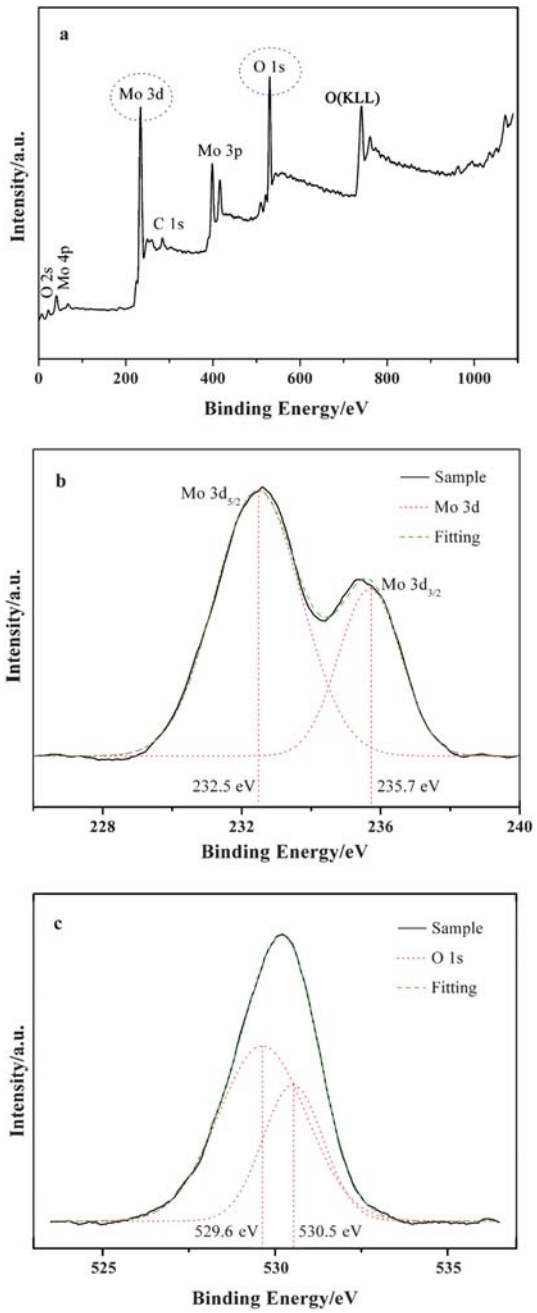

Fig. 5 X-Ray photoelectron spectra of the as-synthesized MoO_3 nanobelts: (a) survey spectrum, (b) Mo 3d spectrum, (c) O 1s spectrum.

MoO_3 phase.[42] The absorption peak at 876 cm^{-1} is attributed to the Mo–O–Mo vibrations of Mo^{6+},[43] which is in good agreement with the XPS analysis. The absorption at 553 cm^{-1} is due to the bending mode vibration of the Mo–O–Mo entity where each O^{2-} ion is shared by three Mo^{6+} ions.[44] The ν(OH) absorption band is very broad with a maximum at 3445 cm^{-1} and is due to O–H stretching of water associated with the powder. The $\delta(H_2O)$ vibrations give an asymmetric band centered at 1630 cm^{-1}, which is ascribed to the bending mode of hydroxyl groups of the adsorbed water in the sample.

Raman spectroscopy is useful in determining the molecular structure of different molybdenum oxide crystal forms, as each of

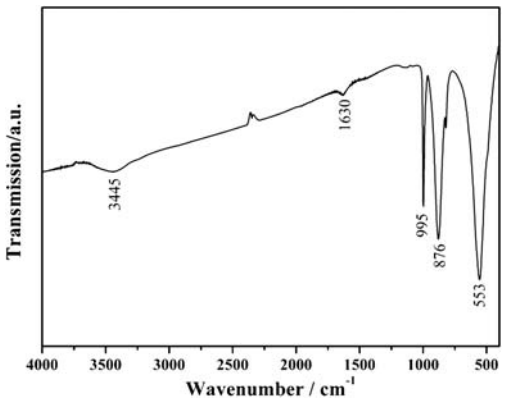

Fig. 6 FT-IR spectrum of the as-synthesized MoO_3 nanobelts.

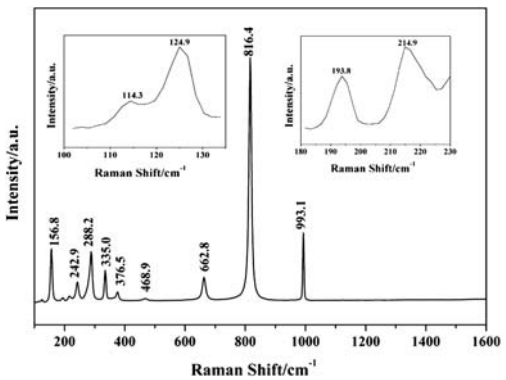

Fig. 7 Raman spectra of the as-synthesized MoO_3 nanobelts.

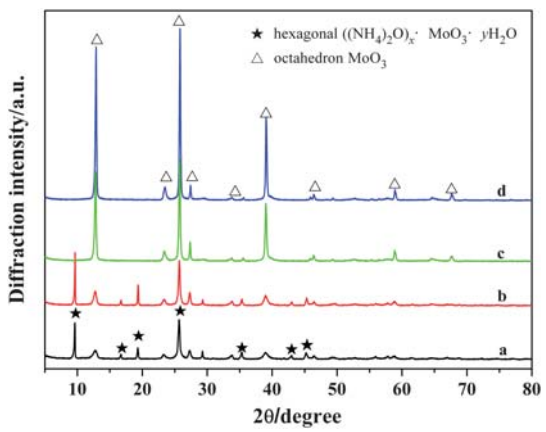

Fig. 8 XRD patterns of the as-prepared products obtained at different reaction time intervals in the presence of TX-10 (reaction temperature = 180 °C): (a) 5 min, (b) 0.5 h, (c) 5 h, (d) 20 h.

them occupies different atomic arrangements and shows quite different Raman vibration bands. The intensity of the Raman peaks varies with the crystal orientation and the polarization of the laser source. The Raman spectra of the as-prepared MoO_3 nanobelts are shown in Fig. 7. The sample shows the typical Raman scattering bands of α-MoO_3, which is in good agreement with those described in refs. 45–48. The bands at 600–1000, 400–600 and below 200 cm^{-1} correspond to the stretching, deformation and lattice modes of α-MoO_3, respectively.

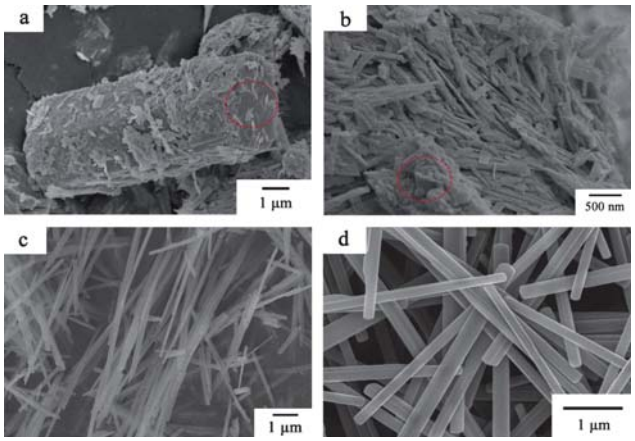

Fig. 9 SEM images of the products collected at different reaction time intervals in the presence of TX-10 (reaction temperature = 180 °C): (a) 5 min, (b) 0.5 h, (c) 5 h, (d) 20 h.

3.2 Growth mechanisms of MoO_3 nanobelts

In order to reveal the growth mechanism of MoO_3 nanobelts, a series of time-dependent experiments were carried out and the intermediate products at different reaction time intervals were then investigated by XRD, SEM, TEM, FT-IR and Raman.

The XRD patterns of the as-prepared products obtained at different reaction times are shown in Fig. 8 and Fig. S1 (ESI†). The products obtained at 5 and 30 min are a mixture of the orthorhombic phase of MoO_3 and hexagonal phase of $((NH_4)_2O)_x \cdot MoO_3 \cdot yH_2O$ (JCPDS 83-1175, $a = 1.053$ nm, $b = 1.053$ nm, $c = 0.373$ nm, space group $P6_3/m$). As the reaction time is prolonged, the products obtained at 90 min and thereafter are pure orthorhombic phase MoO_3.

The SEM images of the as-prepared products obtained at different reaction times are shown in Fig. 9. Two different morphologies can be found in the product obtained at 5 min, *i.e.* nanobelts with width of ~50 nm and length of several hundreds of nm (orthorhombic phase MoO_3), and hexagonal prisms with the side length of ~1 μm (hexagonal phase $((NH_4)_2O)_x \cdot MoO_3 \cdot yH_2O$). A small quantity of the fragments of hexagonal prisms still can be

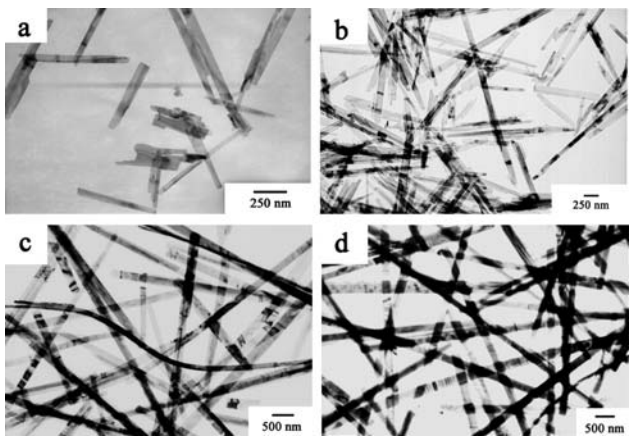

Fig. 10 TEM images of the products collected at different reaction time intervals in the presence of TX-10 (reaction temperature = 180 °C): (a) 5 min, (b) 0.5 h, (c) 5 h, (d) 20 h.

seen in Fig. 9b, although the majority of products obtained at 30 min has the morphology of nanobelts. These results reveal that the products obtained at 5 and 30 min are a mixture of two different phases, which is consistent with the XRD, FT-IR (Fig. S2, ESI†), and Raman results (Fig. S3, ESI†). As the reaction time is further increased to 5 and 20 h, the obtained products show the uniform morphology of nanobelts.

The TEM images of the as-prepared products obtained at different reaction times are shown in Fig. 10. It can be seen that the size of the nanobelts is increased with the reaction time. The width of the nanobelts is increased from ~50 nm to 200–300 nm, and the length of nanobelts is increased from several hundreds of nm to several tens of μm, while the variation of the thickness is negligible. This can be referred to the normal crystallographic dimension of α-MoO_3 in the following sequence: [001] > [100] > [010].[37] Accordingly, the width to length ratio of the nanobelts can be controlled by varying the reaction time.

To further reveal the process of the phase transition, temperature-dependent experiments were carefully carried out, and the products collected after reaction for 20 h were then investigated by XRD. The XRD patterns of the products obtained at different reaction temperatures are shown in Fig. S4 (ESI†). All diffraction peaks of the products obtained at 60 and 80 °C can be indexed to the hexagonal phase of $((NH_4)_2O)_x \cdot MoO_3 \cdot yH_2O$. As the temperature is increased to 100 °C, the characteristic diffraction peaks of the orthorhombic phase of MoO_3 appear and the peak intensity of the hexagonal phase of $((NH_4)_2O)_x \cdot MoO_3 \cdot yH_2O$ is decreased. The products obtained at 120, 140 and 160 °C are indexed to the pure orthorhombic phase of MoO_3. It is revealed that the temperature is very important for the phase transition which occurs with the dehydration process when the temperature is above 100 °C.

Based on the above experimental results, the probable reaction mechanism is presented in Scheme 1. First, the intermediate compound h-$((NH_4)_2O)_x \cdot MoO_3 \cdot yH_2O$ is formed from the starting compound $(NH_4)_6Mo_7O_{24} \cdot 4H_2O$. In the second stage, due to the higher thermal stability of α-MoO_3, when the temperature is above 100 °C, the h-$((NH_4)_2O)_x \cdot MoO_3 \cdot yH_2O$ is dissolved and transformed to α-MoO_3. Then, a further growth and Ostwald ripening lead to the formation of uniform α-MoO_3 nanobelts. This so-called solid–solution–solid crystallization–transformation– recrystallization growth mechanism is very similar with those proposed in refs. 37 and 49.

In addition, in order to study the effect of TX-10, a parallel experiment without the addition of TX-10 was performed under the same conditions. A TEM image of the sample obtained in the absence of TX-10 is shown in Fig. S5 (ESI†). It can be seen that the sample obtained in the absence of TX-10 also has the similar morphology of nanobelts, but the size was not uniform. It is generally believed that the surfactant can be selectively adsorbed on the different crystallographic planes of the nuclei, resulting in

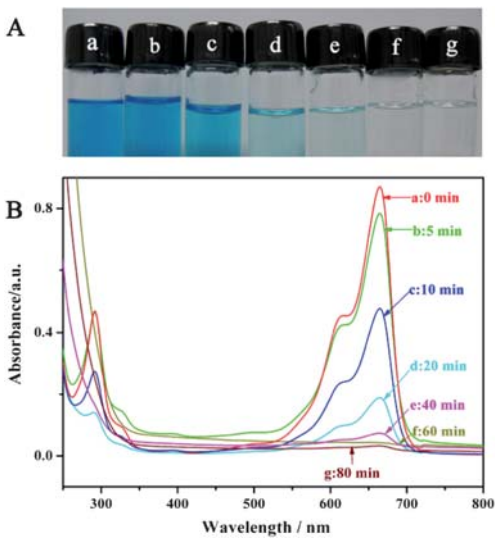

Fig. 11 (A) Photo images and (B) absorption spectra of MB solution (10 mg L^{-1}, 100 mL) in the presence of 50 mg MoO_3 nanobelts at different time intervals.

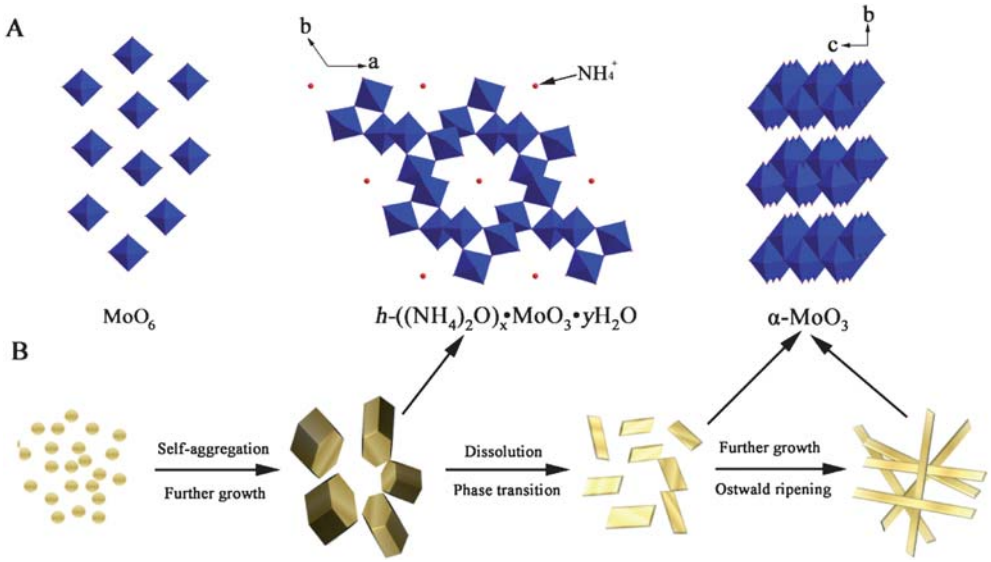

Scheme 1 (A) Crystal structures of h-$((NH_4)_2O)_x \cdot MoO_3 \cdot yH_2O$ and α-MoO_3; (B) The probable growth mechanism of α-MoO_3 nanobelts

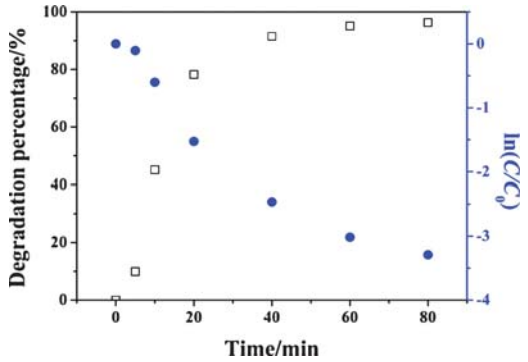

Fig. 12 Degradation percentage of MB (10 mg L^{-1}, 100 mL) in the presence of MoO_3 nanobelts (50 mg) under visible light irradiation.

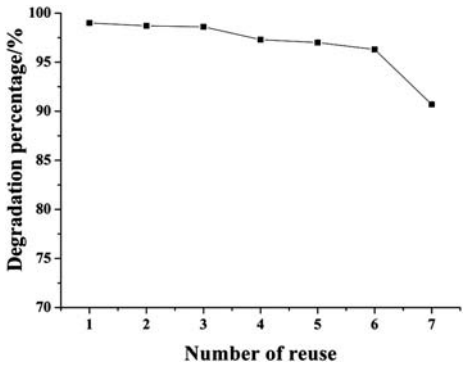

Fig. 13 Cycling runs in the photocatalytic degradation of MB in the presence of MoO_3 nanobelts under visible light irradiation.

the formation of anisotropic nanostructures.[50] Therefore, the formation of α-MoO_3 nanobelts can be regarded as a surfactant-directed growth process, and the presence of TX-10 is important for the synthesis of the uniform α-MoO_3 nanobelts.

3.3 Photocatalytic properties of MoO_3

Photocatalytic performance. The photocatalytic degradation of MB was used as a test reaction to investigate the photocatalytic performance of MoO_3 nanobelts. To eliminate the influence of adsorption, the suspension of MoO_3 nanobelts and MB was magnetically stirred in the dark for 30 min to ensure the adsorption/desorption equilibrium. The equilibrium concentration of MB (C_{eq}) in contact with the catalyst, instead of that of the feed dye solution, was adopted as the true MB concentration at the start of irradiation. The photo images and UV-vis absorption curves of the MB solution at different time intervals are shown in Fig. 11. It can be seen that the intensity of the adsorption peak corresponding to MB at 664 nm decreased with time, in accord with the color fading process. The degradation percentage of MB as a function of time using MoO_3 nanobelts as photocatalyst is shown in Fig. 12. As a contrast, the photocatalytic performance of bulk MoO_3 was also evaluated (Fig. S6 and S7, ESI†). The degradation percentage increased with the irradiation time. Compared with bulk MoO_3, MoO_3 nanobelts show a much higher degradation activity and more than 90% MB can be degraded within 40 min. Three reasons may account for this. First, it is generally accepted that the catalytic process is mainly related to the adsorption and desorption of molecules at the surface of the catalyst. Due to the high specific surface area (MoO_3 nanobelts, 9.3 $m^2 g^{-1}$, bulk MoO_3, 0.45 $m^2 g^{-1}$), the MoO_3 nanobelts possess more unsaturated surface coordination sites which are exposed to the solution. This allows more efficient transport of the reactant molecules to the active sites, and hence the increase of the efficiency of photocatalysis. Second, the high surface-to-volume ratios of nanobelts are in favor of the transfer of electrons and facilitate the degradation of MB. In addition, the good dispersion of MoO_3 nanobelts in the solution is also helpful for maintaining the high active surface area and thus high reaction activity. It is noteworthy that $\ln(C_0/C)$ does not vary linearly with the irradiation time, *i.e.*, the reaction kinetics of MB degradation is not consistent with the pseudo-first order model, which is generally used for the photocatalytic degradation processes if the initial concentration of pollutant is low.[51]

Stability and durability of photocatalysts. The stability of the photocatalyst is crucial to its applications. Most photocatalysts are not stable in the photodegradation process of organic dyes under visible light illumination, and the doped TiO_2 photocatalysts sometimes suffer from this problem.[52,53] To study the stability of the sample, XRD and TEM were performed on the sample before and after photodegradation (Fig. S8 and S9, ESI†). The sample after seven cycles of degradation shows similar diffraction peak positions, which means that the sample still retains the original crystal phase. The marked variation in the relative peak intensity may be due to the surface adsorption of species on the used sample. Moreover, as shown in Fig. S9 (ESI†), the sample still has the similar morphology of nanobelts after seven cycles of degradation. Therefore, the photocatalyst is stable during the reaction and can be used repeatedly. The durability was also studied by re-use of the catalyst in the fresh MB solution under visible light irradiation. Fig. 13 shows the photodegradation results of using the as-obtained MoO_3 nanobelts repeatedly for seven cycles. The MoO_3 nanobelts exhibit a very good durability and there is no significant decrease in the activity even after seven cycles. The degradation percentage of MB still reaches a value of 90.7% even after seven cycles.

3.4 Possible photodegradation mechanism

It is widely accepted that there are three possible processes for the photodegradation of dye over a semiconductor, *i.e.* a photocatalytic process, a dye photo-sensitization process, or a photolysis process.[54–57] For the photocatalytic process, photo-induced electrons and holes existing over a semiconductor directly or indirectly react with O_2 and OH^- to form active oxidants $^{\bullet}O_2^-$ and $^{\bullet}OH^-$, respectively. For the photosensitization process of dye, photo-induced electrons in the dye transfer to the conduction band of the catalyst that absorbs the dye, and subsequently react with molecular oxygen to produce the $^{\bullet}O_2^-$ oxidant. The photolysis of dye originates from the destruction of a dye upon photoirradiation, which is closely related to the structural stability of the dye. In our experiment, the degradation of MB under visible light without the photocatalyst is not observable. This means that MB shows a high structural stability and the

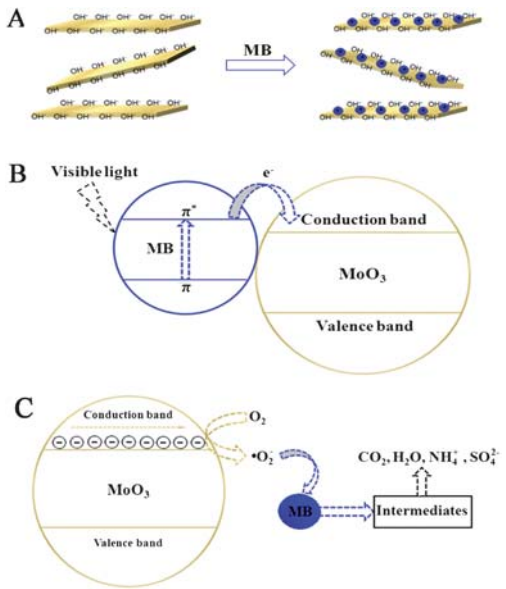

Scheme 2 Possible mechanism for the photodegradation of MB under visible light. (A) MB is absorbed at the surface of α-MoO_3 nanobelts; (B) MB absorbs visible light to induce the π–π* transition, the excited-state electrons then readily inject into the d-orbital (CB) of MoO_3; (C) the excited-state electrons react with adsorbed oxygen to yield superoxide radicals $^{\bullet}O_2^-$ and then MB is mineralized by the radicals.

degradation of MB *via* the photolysis mechanism is negligible. In other words, the degradation of MB is mainly initiated by a photocatalytic process or a dye photosensitization process.

In order to investigate the role of the photosensitization in the total decolorization of MB, the UV/vis reflectance spectroscopy of the as-obtained α-MoO_3 nanobelts was tested (Fig. S10, ESI†). It is revealed that the α-MoO_3 nanobelts have a band gap of ~ 3.01 eV and can not respond to visible light of $\lambda > 420$ nm. Thus, it is believed that the photosensitization process plays a key role in the degradation of MB.

A zeta-potential test is an effective way for the characterization of the surface charge. It was found that the MoO_3 nanobelts were negatively charged at neutral pH with a ζ-potential of −34.5 mV. The negative value of the ζ-potential can be explained by an excess of OH^- absorbed on the particle surface. On the other hand, after magnetically stirring in the dark for 30 min, the suspension of MoO_3 nanobelts and MB was positively charged at neutral pH with a ζ-potential of +28.7 mV.

Based on the results of photodegradation and ζ-potential tests, and enlightened by the reported ref. 58, a self-sensitized photocatalytic mechanism under visible light irradiation can be proposed as shown in Scheme 2. First, MB is absorbed at the surface of MoO_3 nanobelts *via* electrostatic interaction. MB absorbs visible light to induce the π–π* transition, transporting the excited-state electrons to the π*-orbital. In the excited state, the dye ejects one electron to the d-orbital (CB) of MoO_3 and this is subsequently transferred to the surface to react with the adsorbed oxygen to yield superoxide radicals $^{\bullet}O_2^-$. These surface radicals can act as effective centers for the photocatalytic reactions. Organic compounds, such as MB, are believed to be mineralized through the direct oxidation by the radicals.[6] More experiments should be performed to further study the intermediate products and the mineralization process.

4. Conclusion

In conclusion, MoO_3 nanobelts with widths of 200–300 nm and lengths of several tens of micrometres were obtained through a simple and mild hydrothermal route with the assistance of TX-10. Based on the time-dependent experiments, a solid–liquid–solid transformation mechanism was proposed for the formation of α-MoO_3 nanobelts. The photocatalytic measurements showed that the α-MoO_3 nanobelts had a high activity and very good stability for the degradation of organic dyes such as MB under visible light irradiation, making them a promising candidate for practical photocatalysts. A self-sensitization photocatalytic process was suggested for the first time based on the experiment results. Further study investigating the detailed photocatalytic mechanism, and hence to improve the photocatalytic properties of α-MoO_3, is under way in our lab.

Acknowledgements

This work was financially supported by the National Natural Science Foundation of China (20773065, 20635020), the Project of Environmental Protection Department from Jiangsu Province, China (2008003), and National Basic Research Program (973 project) (2007CB936302). The authors acknowledge the Modern Analysis Center of Nanjing University for characterization assistance.

References

1 A. Fujishima and K. Honda, *Nature*, 1972, **238**, 37.
2 M. R. Hoffmann, S. T. Martin, W. Y. Choi and D. W. Bahnemann, *Chem. Rev.*, 1995, **95**, 69.
3 Z. G. Zou, J. H. Ye, K. Sayama and H. Arakawa, *Nature*, 2001, **414**, 625.
4 H. Kominami, S. Murakami, J. Kato, Y. Kera and B. Ohtani, *J. Phys. Chem. B*, 2002, **106**, 10501.
5 J. C. Yu, L. Z. Zhang, Z. Zheng and J. C. Zhao, *Chem. Mater.*, 2003, **15**, 2280.
6 H. Zhang, R. L. Zong, J. C. Zhao and Y. F. Zhu, *Environ. Sci. Technol.*, 2008, **42**, 3803.
7 L. W. Zhang, H. B. Fu and Y. F. Zhu, *Adv. Funct. Mater.*, 2008, **18**, 2180.
8 S. Banerjee, S. K. Mohapatra, P. P. Das and M. Misra, *Chem. Mater.*, 2008, **20**, 6784.
9 X. K. Li, N. Kikugawa and J. H. Ye, *Adv. Mater.*, 2008, **20**, 3816.
10 Y. Ebina, T. Sasaki, M. Harada and M. Watanabe, *Chem. Mater.*, 2002, **14**, 4390.
11 T. Nakato and Y. Matsumoto, *J. Porous Mater.*, 2004, **11**, 79.
12 N. Miyamoto and T. Nakato, *J. Phys. Chem. B*, 2004, **108**, 6152.
13 T. G. Xu, C. Zhang, X. Shao, K. Wu and Y. F. Zhu, *Adv. Funct. Mater.*, 2006, **16**, 1599.
14 Y. B. Li, Y. Bando, D. Golberg and K. Kurashima, *Appl. Phys. Lett.*, 2002, **81**, 5048.
15 X. L. Li, J. F. Liu and Y. D. Li, *Appl. Phys. Lett.*, 2002, **81**, 4832.
16 G. R. Patzke, A. Michailovski, F. Krumeich, R. Nesper, J. D. Grunwaldt and A. Baiker, *Chem. Mater.*, 2004, **16**, 1126.
17 Z. Hussain, *J. Mater. Res.*, 2001, **16**, 2695.
18 J. N. Yao, K. Hashimoto and A. Fujishima, *Nature*, 1992, **355**, 624.
19 Y. A. Yang, Y. W. Cao, B. H. Loo and J. N. Yao, *J. Phys. Chem. B*, 1998, **102**, 9392.
20 A. M. Taurino, A. Forleo, L. Francioso, P. Siciliano, M. Stalder and R. Nesper, *Appl. Phys. Lett.*, 2006, **88**, 152111.
21 H. F. Liu, R. S. Liu, K. Y. Liew, R. E. Johnson and J. H. Lunsford, *J. Am. Chem. Soc.*, 1984, **106**, 4117.

22 T. Itoh, I. Matsubara, W. Shin, N. Izu and M. Nishibori, *Sens. Actuators, B*, 2008, **128**, 512.
23 J. Song, X. M. Ni, D. Zhang and H. G. Zheng, *Solid State Sci.*, 2006, **8**, 1164.
24 T. He and J. N. Yao, *J. Photochem. Photobiol., C*, 2003, **4**, 125.
25 X. L. Li and Y. D. Li, *Chem.–Eur. J.*, 2003, **9**, 2726.
26 W. K. Hsu, B. H. Chang, Y. Q. Zhu, W. Q. Han, H. Terrones, M. Terrones, N. Grobert, A. K. Cheetham, H. W. Kroto and D. R. M. Walton, *J. Am. Chem. Soc.*, 2000, **122**, 10155.
27 Y. Feldman, E. Wasserman, D. J. Srolovitz and R. Tenne, *Science*, 1995, **267**, 222.
28 M. Hershfinkel, L. A. Gheber, V. Volterra, J. L. Hutchison, L. Margulis and R. Tenne, *J. Am. Chem. Soc.*, 1994, **116**, 1914.
29 M. P. Zach, K. H. Ng and R. M. Penner, *Science*, 2000, **290**, 2120.
30 K. Nina, Y. Kimura, K. Yokoyama, O. Kido, G. Binyo and C. Kaito, *Phys. E.*, 2008, **40**, 2995.
31 C. V. S. Reddy, E. H. Walker, C. Wen and S. I. Mho, *J. Power Sources*, 2008, **183**, 330.
32 B. G. Qi, X. M. Ni, D. G. Li and H. G. Zheng, *Chem. Lett.*, 2008, **37**, 336.
33 L. Fang, Y. Y. Shu, A. Q. Wang and T. Zhang, *J. Phys. Chem. C*, 2007, **111**, 2401.
34 S. T. Wang, Y. G. Zhang, X. C. Ma, W. Z. Wang, X. B. Li, Z. D. Zhang and Y. T. Qian, *Solid State Commun.*, 2005, **136**, 283.
35 Z. H. Wen, Q. Wang and J. H. Li, *J. Nanosci. Nanotechnol.*, 2006, **6**, 2117.
36 L. Cheng, M. W. Shao, X. H. Wang and H. B. Hu, *Chem.–Eur. J.*, 2009, **15**, 2310.
37 X. W. Lou and H. C. Zeng, *Chem. Mater.*, 2002, **14**, 4781.
38 M. Epifani, P. Imperatori, L. Mirenghi, M. Schioppa and P. Siciliano, *Chem. Mater.*, 2004, **16**, 5495.
39 T. A. Xia, Q. Li, X. D. Liu, J. A. Meng and X. Q. Cao, *J. Phys. Chem. B*, 2006, **110**, 2006.
40 N. S. Ramgir, D. J. Late, A. B. Bhise, M. A. More, I. S. Mulla, D. S. Joag and K. Vijayamohanan, *J. Phys. Chem. B*, 2006, **110**, 18236.
41 J. D. Ye, S. L. Gu, F. Qin, S. M. Zhu, S. M. Liu, X. Zhou, W. Liu, L. Q. Hu, R. Zhang, Y. Shi, Y. D. Zheng and Y. D. Ye, *Appl. Phys. A: Mater. Sci. Process.*, 2005, **81**, 809.
42 S. Morandi, G. Ghiotti, A. Chiorino and E. Comini, *Thin Solid Films*, 2005, **490**, 74.
43 W. Dong and B. Dunn, *J. Mater. Chem.*, 1998, **8**, 665.
44 G. A. Nazri and C. Julien, *Solid State Ionics*, 1992, **53–56**, 376.
45 S. Phadungdhitidhada, P. Mangkorntong, S. Choopun and N. Mangkorntong, *Ceram. Int.*, 2008, **34**, 1121.
46 D. Liu, W. W. Lei, J. Hao, D. D. Liu, B. B. Liu, X. Wang, X. H. Chen, Q. L. Cui, G. T. Zou, J. Liu and S. Jiang, *J. Appl. Phys.*, 2009, **105**, 023513.
47 M. Dieterle and G. Mestl, *Phys. Chem. Chem. Phys.*, 2002, **4**, 822.
48 L. G. Pereira, L. E. B. Soledade, J. M. Ferreira, S. J. G. Lima, V. J. Fernandes, A. S. Araujo, C. A. Paskocimas, E. Longo, M. R. C. Santos, A. G. Souza and I. M. G. Santos, *J. Alloys Compd.*, 2008, **459**, 377.
49 J. Nyvlt, *Cryst. Res. Technol.*, 1997, **32**, 695.
50 S. F. Shi, M. H. Cao, X. Y. Fle and H. M. Xie, *Cryst. Growth Des.*, 2007, **7**, 1893.
51 M. Sleiman, P. Conchon, C. Ferronato and J. M. Chovelon, *Appl. Catal., B*, 2007, **71**, 279.
52 J. J. He, A. Hagfeldt, S. E. Lindquist, H. Grennberg, F. Korodi, L. C. Sun and B. Akermark, *Langmuir*, 2001, **17**, 2743.
53 E. Bae and W. Choi, *Environ. Sci. Technol.*, 2003, **37**, 147.
54 C. Nasr, K. Vinodgopal, L. Fisher, S. Hotchandani, A. K. Chattopadhyay and P. V. Kamat, *J. Phys. Chem.*, 1996, **100**, 8436.
55 X. P. Lin, F. Q. Huang, W. D. Wang, Y. M. Wang, Y. J. Xia and J. L. Shi, *Appl. Catal., A*, 2006, **313**, 218.
56 C. G. da Silva and J. L. Faria, *J. Photochem. Photobiol., A*, 2003, **155**, 133.
57 A. Houas, H. Lachheb, M. Ksibi, E. Elaloui, C. Guillard and J. M. Herrmann, *Appl. Catal., B*, 2001, **31**, 145.
58 D. Chatterjee and S. Dasgupta, *J. Photochem. Photobiol., C*, 2005, **6**, 186.